nature portfolio

Peer Review File

A General Flame Aerosol Route to Kinetically Stabilized Metal-Organic Frameworks

Corresponding Author: Professor Mark Swihart

Version 0:

Reviewer comments:

Reviewer #1

(Remarks to the Author)
This manuscript reports a general and versatile non-equilibrium flame aerosol synthesis of MOFs, in which rapid kinetics of MOF formation yields two distinct classes of MOFs, nano-crystalline MOFs and amorphous MOFs. This work is interesting. I recommend the acceptance of this manuscript after addressing the following issues.
1. How to accurately control the reaction temperature in the preparation process ?
2. Can the quality of the product be given in Figure S1?
3. The statistical software of particle size distribution diagram in Figure S2 should be given.
4. There is an obvious diffraction peak in Figure 3(B). How to explain it is amorphous material?
5. Can the product with smaller particle size be prepared with lower concentration?

Reviewer #2

(Remarks to the Author)
This article describes a new Metal-Organic Framework synthetic way based on the fast drying of an aerosol generated at high temperature. The application of this synthetic strategy on MOFs is completely new and very interesting, with many potential applications ranging from the synthesis of MOFs at large scale to their functionalization, for example for catalysis, as evidenced in the last part of the article. The article is well-written and I find the topic very interesting for a publication in Nature Communications but several point must be addressed prior to any publication:
1/ The description of the synthetic process is not really detailed and it is a bit hard to understand how all the parameters (nature of the solvent, concentration of reactants, gaz flux, temperature…) have been chosen and what is their impact on the properties of the obtained solid. The authors should clarify this point.
2/ The washing/activation procedure is a key step of the MOF synthesis. How did the author select the solvents for washing (DMF and MeOH)? In addition, more quantitative information on the washing must be provided (time, temperature, solvent volume…). After washing, what is the synthesis yield of the different MOFs obtained?
3/ For the part concerning crystalline MOFs, can the author justify the choice of MOFs they made (especially because some of them are not “benchmarck” materials for the MOF community)? How can this technique be extended to other MOFs? Can the authors suggest parameters (nature of the metal cation? Of the linker? Solubility ? …) to make the synthesis of crystalline MOF successful or not?
4/ Concerning the part dealing with amorphous MOF, I would like to emphasize that any powder containing a metal cation and a linker cannot be considered as an amorphous MOF but that some reminiscence of the MOF properties should be evidenced on the amorphous solid (stoichiometry, local order, porosity…) to be considered as an amorphous MOF. For example, when dealing with Zr FMA (Figure 3), the PDF data given on Figure 3C should be modelled or compared with the theoretical one for the crystalline solid in order to see what does the signal account for. In particular, in the context of Zr MOFs, is it possible to see if Zr6 oxoclusters are formed in the amorphous solid? Moreover, the TGA in Figure 3E must be analyzed to evaluated the amount of FMA linker in the amorphous solid and see how it compares with the stoichiometry of the parent crystalline solid.
5/ Similar questions must be discussed for the other compounds (Zr UiO-66-NH2, Fe FMA, 227 Mg DHTA, Cu DHTA, Zr BTC, Zr BPDC, Fe BDC-NH2 and Hf NDC). Giving the PXRD of the amorphous solids and electron microscopy images of the particles is clearly not enough to claim the synthesis of an amorphous MOF.
6/ Authors claim that they can control the amount of Au, Co, Pt, and Pd loaded in the different MOFs but how does the amount of metal cations loaded determined by ICP compare with the expected one. Moreover, did the authors optimize the washing of the doped solids? Did they observe any metal leaching during the washing procedure?
7/ Finally, the authors should carefully check the reference list. Some of them seems to be completely unrelated to the citation. For exemple « Additionally, the particular surface characteristics of these nano-crystals may lead to enhanced reactivity and selectivity in chemical reactions” is not related to reference 18 “Introduction to metal-organic frameworks” that

is a very broad introduction on MOFs and “Moreover, the higher concentration of structural defects in nano-crystalline MOFs can be beneficial.” is not related to reference 19 whose title is “Weaving of organic threads into a crystalline covalent organic framework” that deals with COFs and not MOFs.

Reviewer #3

(Remarks to the Author)
The manuscript describes the non-equilibrium gas phase synthesis of crystalline/non-crystalline metal organic framework architectures. I find this process idea fascinating and worth publishing in nature communications. The success of this technique would significantly contribute to the synthesis of these classes of materials that are possible only via multiple chemical routes as shown in scheme 1. However, before this manuscript can be published, there are some critical chemical engineering issues during synthesis that need to be clarified.

1. The H2 and O2 combustion in an inverted diffusion flame was realized with additional 10L/min N2-Co flow to cool down the flame. While the stoichiometry of H2/O2 ratio for complete combustion is 1/0.5 [H2 + 0.5O2 H2O + (-470kJ/mol)], the ratio used in the manuscript is 1/1.14 (3.5LH2/4LO2 min-1), i.e. highly O2 rich environment. The reaction is exothermic with extra surplus oxygen. As authors suggested, the temperature of the reactor is maintained at 400°C is highly unlikely due to easy exothermic oxidation resulting to more heat generation in the reaction vicinity. As shown in figure 1, the high flow of N2 (140L/min) would cool down the aerosol stream but the high temperature in the reaction zone would decompose the precursor components, that depends on flame top -precursor entry point distance. What is the distance from the top of the flame to the precursor entry point? If the aerosol stream is already around 400°C, why is there a need of such a high N2 co-flow?

2. The components for Cu-based MOF (CuHKUST-1) described in the text are Cu(NO3)2 and 1,3,5-benzenetricarboxylic acid, DMF, EtOH, and H2O.
• Out of these components, Cu(NO3)2 decomposes at 400°C. In this case, how would Cu be incorporated in the organic framework?
• 1,3,5-benzenetricarboxylic acid, DMF, EtOH decompose at 250, 350 and 78°C, i.e. each component has different temperature of decomposition. While the process is very rapid, how would the time be sufficient for different decomposition components followed by the MOF formation?

Version 1:

Reviewer comments:

Reviewer #1

(Remarks to the Author)
All issues have been well addressed point by point. It can be accepted for publication in Nature Communications.

Reviewer #2

(Remarks to the Author)
The authors satisfactory took into account all the issues raised in my previous report. Therefore, I recommend the publication of the manuscript in its current form.

Reviewer #3

(Remarks to the Author)
The manuscript describing the non-equilibrium gas phase synthesis of crystalline/non-crystalline metal organic framework architectures has been nicely revised. The reviewer questions (from all the three) from the manuscript are well clarified. I believe that this manuscript is now ready for the publication in nature communications.
One last question: Authors claim “HNO3 (as a byproduct) evaporates along with the solvents”.
• What is the boiling point difference between nitric acid and the other solvents?
• Does HNO3 decompose during the process?
• What are the safety issues for non-exposure conditions to the environment?

Please clarify this in the final version.

Response to Reviewer #1's comments:

Reviewer #1 (Remarks to the Author):

This manuscript reports a general and versatile non-equilibrium flame aerosol synthesis of MOFs, in which rapid kinetics of MOF formation yields two distinct classes of MOFs, nano-crystalline MOFs and amorphous MOFs. This work is interesting. I recommend the acceptance of this manuscript after addressing the following issues.

We thank the Reviewer for the positive comments!

1. How to accurately control the reaction temperature in the preparation process?

Our response: During the reaction process, the adiabatic flame temperature can be controlled by adjusting the gas flow rates, which in turn allows for the control over the reaction temperature. In the synthesis of MOFs reported here, we can precisely control the reaction temperature by modulating the H_2 gas flow rate.

Based on the Reviewer's suggestion, we have added the following explanation in the synthesis section:

The reaction temperature can be controlled by modulating the H_2 gas flow rate, which determines the total heat release in the flame, *i.e.*, the adiabatic flame temperature.

2. Can the quality of the product be given in Figure S1?

Our response: The production yield of MOFs in the current laboratory-scale reactor ranges from 0.3 to 1 g/h. If an industrial-scale reactor is established, the production rate will be significantly increased. Following the Reviewer's suggestion, we have included this yield in Figure S1 to demonstrate the potential scale-up benefits of an industrial-scale reactor,

The current laboratory-scale reactor produces MOFs at a yield ranging from 0.3 to 1 g/h.

3. The statistical software of particle size distribution diagram in Figure S2 should be given.

Our response: Based on the Reviewer's suggestion, we have included the statistical software

used for determination of particle size distribution in Figure S2 and Figure S10 as follows:

The particle size distribution was analyzed using ImageJ software.

4. There is an obvious diffraction peak in Figure 3(B). How to explain it is amorphous material?

Our response: In general, "amorphous" is not a rigorously defined term in materials science, and may be interpreted differently in different fields (*e.g.,* polymer science vs. metallurgy). As commonly used in inorganic materials, including porous frameworks like MOFs, "amorphous" materials do not lack organization altogether; rather they exhibit short-range order but lack long-range crystalline periodicity. Thus, they often exhibit a broad peak in XRD (*e.g.*, *Science 367.6485 (2020): 1473-1476.; Journal of the American Chemical Society 138.34 (2016): 10818-10821; Nature communications (2021) 12:2062*). This is the case for the peak observed in Figure 3(B).

To illustrate this point, we have referenced similar broad XRD diffraction peaks observed in other reported amorphous MOFs to the manuscript,

Similar broad XRD diffraction peaks have also been observed in other reported amorphous MOFs.[21,37,38]

The mentioned papers are also added in the references:

21. Madsen, R.S. et al. Ultrahigh-field 67Zn NMR reveals short-range disorder in zeolitic imidazolate framework glasses. *Science* **367**, 1473-1476 (2020).

37. Zhao, Y., Lee, S.Y., Becknell, N., Yaghi, O.M. & Angell, C.A. Nanoporous Transparent MOF Glasses with Accessible Internal Surface. *J. Am. Chem. Soc.* **138**, 10818-21 (2016).

38. Sapnik, A.F. et al. Mixed hierarchical local structure in a disordered metal-organic framework. *Nat. Commun.* **12**, 2062 (2021).

The short range order of this material is further revealed by pair distribution function (PDF) analysis. As shown in Figure 3C, the PDF pattern shows major peaks below 5 Å, corresponding to the distances between nearest neighbor atom pairs. Notably, there are no evident peaks at medium-range or longer distances. This PDF pattern is comparable to those of other reported amorphous MOFs (***e.g., Nature Materials 22.7 (2023): 888-894; Physical Review Letters 104.11 (2010): 115503***).

We have also added the comparison in the manuscript as follows:

Similar PDF patterns revealing short-range order were observed for other reported amorphous

MOFs.[23,39]

The mentioned papers have also been added in the references:

23. Yang, Z. et al. ZIF-62 glass foam self-supported membranes to address CH_4/N_2 separations. *Nat. Mater.* **22**, 888-894 (2023).

39. Bennett, T.D. et al. Structure and properties of an amorphous metal-organic framework. *Phys. Rev. Lett.* **104**, 115503 (2010).

5. Can the product with smaller particle size be prepared with lower concentration?

Our response: Based on the Reviewer's suggestion, we measured the particle size of MOFs synthesized from low concentration precursors. The previously measured crystalline Cu HKUST-1 and amorphous Zr FMA MOFs were synthesized using 20 mM metal ion precursors. We synthesized crystalline Cu HKUST-1 MOFs and amorphous Zr FMA MOFs with lower metal concentrations of 5 mM and 10 mM in the precursor solutions. The particle size of MOFs synthesized from different precursor concentrations (5 mM, 10 mM, and 20 mM) were measured. As expected, products with smaller particle size were prepared using lower precursor concentrations.

We have added the particle size data for crystalline Cu HKUST-1 MOFs synthesized from different Cu ion concentrations in **Fig. S2** as follows:

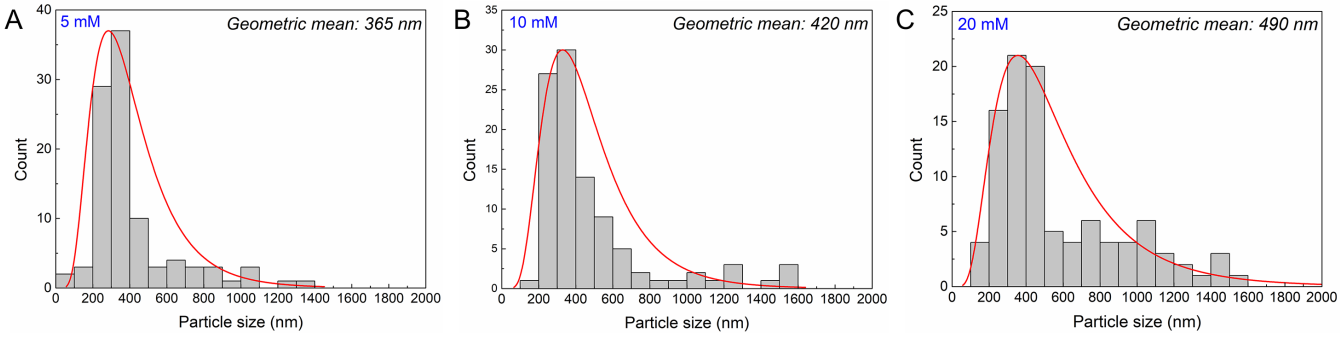

Fig. S2. Particle size distribution of crystalline Cu HKUST-1 MOFs synthesized using **A.** 5 mM, **B.** 10 mM, and **C.** 20 mM Cu ion precursors, based on statistics of 100 particles in SEM images. The particle size distribution was analyzed using ImageJ software.

In the Manuscript, we have added the explanation as follows:

A series of Cu HKUST-1 MOFs prepared from precursors containing 5 mM, 10 mM, and 20 mM Cu ions under otherwise identical conditions exhibited geometric mean diameters of 365 nm, 420 nm, and 490 nm, respectively, demonstrating that the particle size can tuned to some degree by varying the concentration of the precursor (**Fig. S2**).

We have also added the particle size of amorphous Zr FMA MOFs synthesized from different Zr ion concentrations in **Fig. S10** as follows:

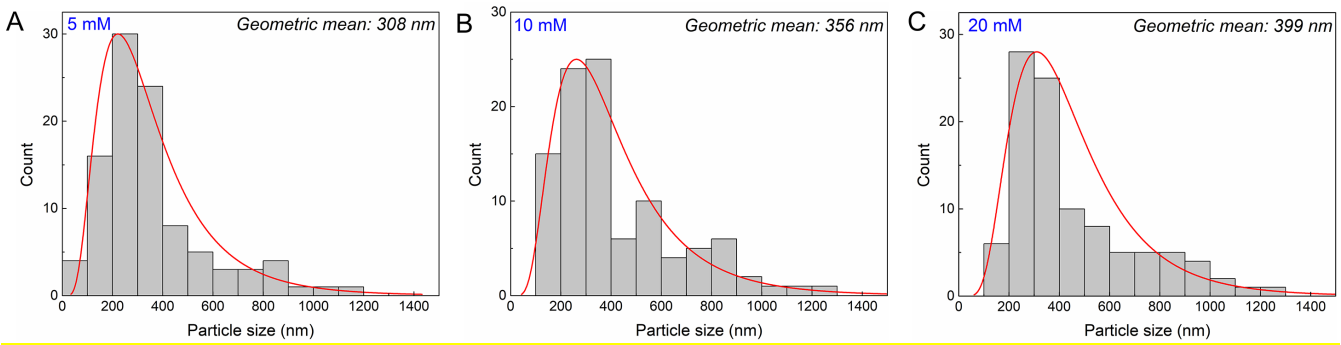

Fig. S10. Particle size distribution of amorphous Zr FMA MOFs synthesized using **A.** 5 mM, **B.** 10 mM, and **C.** 20 mM Zr ion precursors, based on statistics of 100 particles in SEM images. The particle size distribution was analyzed using ImageJ software.

In the Manuscript, we have added the explanation as follows:

A series of amorphous Zr FMA MOFs prepared from precursors containing 5 mM, 10 mM, and 20 mM Zr ions under otherwise identical conditions exhibited geometric mean diameters of 308 nm, 356 nm, and 399 nm, respectively (**Fig. S10**).

Response to Reviewer #2's comments:

Reviewer #2 (Remarks to the Author):

This article describes a new Metal-Organic Framework synthetic way based on the fast drying of an aerosol generated at high temperature. The application of this synthetic strategy on MOFs is completely new and very interesting, with many potential applications ranging from the synthesis of MOFs at large scale to their functionalization, for example for catalysis, as evidenced in the last part of the article. The article is well-written and I find the topic very interesting for a publication in Nature Communications but several point must be addressed prior to any publication:

We thank the Reviewer for the positive comments!

1/ The description of the synthetic process is not really detailed and it is a bit hard to understand how all the parameters (nature of the solvent, concentration of reactants, gas flux, temperature…) have been chosen and what is their impact on the properties of the obtained solid. The authors should clarify this point.

Our response: In this research, we present the synthesis of over 20 different MOFs. The liquid-phase synthesis of MOFs is known to be influenced by numerous reaction parameters that affect properties including morphology, crystallinity, and porosity, which can be tuned to meet specific application needs by tailored synthesis methods. Similarly, the flame aerosol synthesis method introduced in this study could be carefully optimized for each of the MOFs and to meet specific application needs. However, to demonstrate the versatility of this new method, we standardized the flame synthesis conditions and washing procedures across all MOFs. Our aim was to employ general reaction parameters suitable for synthesizing all featured MOFs. For instance, to prevent precursor ignition, we ensured that all solvents contained ~60% water. We have included a limited amount of parameter variation, such as showing that lower precursor concentrations reduce the particle size. However, exploring the effects of reaction conditions on the properties of each of these 20 MOFs was not the primary focus of this study.

Fortunately, like liquid-phase synthesis, the reaction parameters in flame aerosol synthesis can be flexibly adjusted to customize the properties of MOFs to meet various application needs. For example, in this study, we have shown that the particle size and porosity of the flame-

synthesized MOFs can be controlled by adjusting the metal concentration in the precursors (**Fig. S2, Fig. S10, Table S3**). Additionally, the catalytic performance of the MOF tested for CO oxidation reaction can be optimized by modifying the Pt content (**Fig. S5E**). In future research, we plan to precisely design the structure and properties of specific MOF based on application requirements.

Based on the Reviewer's suggestion, we have added the detailed explanation in the Results and Discussion section as follows:

… The fast evaporation and resulting solute concentration increase inherent in the flame aerosol process promotes rapid MOF formation. This can either occur through simultaneous nucleation of multiple crystalline domains within each droplet or result in a disordered framework. The rapid droplet-to-particle conversion in this process typically yields kinetic, rather than thermodynamic, products. In this context, two distinct classes of MOFs, nano-crystalline MOFs and amorphous MOFs can be produced (**Fig. 1**). The product properties can be varied and optimized by adjusting reaction parameters (*e.g.*, gas flow rates, H_2 to O_2 ratio, precursor flow rate, precursor concentration, and metal ion to linker ratio). However, in this study, to demonstrate the versatility of the method, all MOFs were synthesized using a common set of synthesis and washing procedures, with only the precursor composition varying (**Table S1, S2**).

Meanwhile, further details of the synthetic process were added in the Methods section:

…To prevent the precursor solution from igniting, a mixture of organic solvent and water was used as the solvent ensure solubility of all precursor components without using a flammable solvent mixture. The ratio of metal cations to organic ligands in the precursor was selected based on typical MOF structures and conventional synthesis methods. For example, in the synthesis of Cu HKUST-1 ($Cu_3(BTC)_2$), $Cu(NO_3)_2$ and 1,3,5-benzenetricarboxylic acid in a 3:2 molar ratio were dissolved in a mixture of DMF, EtOH, and H_2O. In the flame reactor, an inverted diffusion flame was generated by igniting a gas mixture of 3.5 L/min H_2, 10 L/min N_2, and 4 L/min O_2, yielding a temperature of ~400 ºC in the reactor chamber. The reaction temperature can be varied by increasing or decreasing the H_2 gas flow rate…

2/ The washing/activation procedure is a key step of the MOF synthesis. How did the author select the solvents for washing (DMF and MeOH)? In addition, more quantitative information on the washing must be provided (time, temperature, solvent volume…). After washing, what is the synthesis yield of the different MOFs obtained?

Our response: To demonstrate the versatility of this new method, we applied a standard washing procedure to all MOFs, as outlined in ***Chemical Society Reviews 49.20 (2020): 7406-7427***. First, DMF is employed to remove any residual metals and organic ligands from the MOFs, then methanol (a high vapor pressure solvent) is used to replace the less volatile DMF. Note that these washing and activation procedures can be tailored and optimized depending on the specific type and requirements of each MOF. Currently, the yield of MOFs in our laboratory-scale reactor (MOF product per hour of reactor operation, after washing) ranges from 0.3 to1 g/h. Establishing an industrial-scale reactor could significantly enhance the MOF yield.

Based on the Reviewer's suggestion, we have added the detailed description of the washing procedures and MOF yields in the Method section as follows:

The produced powder was re-dispersed in 30 mL solvent, sonicated for 1 hour, and soaked for over 5 hours at room temperature before being centrifuged. It was washed twice with DMF and once with methanol. Finally, the sample was vacuum-dried at 60 ºC overnight. The production yield of MOFs is 0.3~1 g of washed product per hour of reactor operation.

3/ For the part concerning crystalline MOFs, can the author justify the choice of MOFs they made (especially because some of them are not "benchmarck" materials for the MOF community)? How can this technique be extended to other MOFs? Can the authors suggest parameters (nature of the metal cation? Of the linker? Solubility? …) to make the synthesis of crystalline MOF successful or not?

Our response: When designing MOFs to demonstrate the versatility of our method, we used a variety of organic ligands and metals. This study represents the first exploration of synthesizing MOFs with this technique. Instead of designing a specific MOF intentionally, we focused on exploring diverse possibilities to evaluate the potential of our approach. This method can be adapted to other MOFs by selecting different metals and organic linkers. Due to variations in reaction kinetics compared to traditional liquid-phase methods, this approach has the potential to yield many novel MOFs. We believe that this method and the new synthesis concept proposed here hold immense potential for future exploration. Thus, we included examples of well-studied MOFs (Cu HKUST-1, which exhibited the typical crystal structure, and UiO-66-NH_2 which was produced in amorphous form) but believe the greater impact of our approach will be for less-studied or previously unreported MOFs.

In the materials we have explored so far, we found that transition metals such as Cu, Zn, and

Ni readily form crystalline MOFs. Meanwhile, the formation of MOF crystals is influenced by the evaporation rate of the precursor droplets; slower droplet evaporation provides more time for MOF nucleation and growth, facilitating the assembly of MOFs into crystals. Therefore, we speculate that methods to slow the evaporation rate, such as lowering the reaction temperature, may enhance the formation of crystalline MOFs. However, as the Reviewers noted, this also depends largely on the type of MOF, as well as factors such as reactant concentration and solvent choice, all of which are currently under investigation.

Based on the Reviewer's suggestion, we propose the following parameters to optimize the production of crystalline MOFs:

In our exploration of MOF synthesis, we observed that metals like Cu, Zn, and Ni tend to form crystalline MOFs more readily. The assembly of MOFs depends on the evaporation rate of the precursor droplets. Methods that decelerate this evaporation, such as reducing the reaction temperature, may favor the formation of crystalline MOFs.

4/ Concerning the part dealing with amorphous MOF, I would like to emphasize that any powder containing a metal cation and a linker cannot be considered as an amorphous MOF but that some reminiscence of the MOF properties should be evidenced on the amorphous solid (stoichiometry, local order, porosity…) to be considered as an amorphous MOF. For example, when dealing with Zr FMA (Figure 3), the PDF data given on Figure 3C should be modelled or compared with the theoretical one for the crystalline solid in order to see what does the signal account for. In particular, in the context of Zr MOFs, is it possible to see if Zr_6 oxoclusters are formed in the amorphous solid? Moreover, the TGA in Figure 3E must be analyzed to evaluated the amount of FMA linker in the amorphous solid and see how it compares with the stoichiometry of the parent crystalline solid.

Our response:

We appreciate this insight from the Reviewer, and have attempted to provide a clearer presentation of the evidence, from several perspectives, which we believe demonstrates that the flame synthesized Zr FMA is an amorphous MOF. As noted by the Reviewer, the PDF data provide key evidence. Based on the Reviewer's suggestion, we compared our PDF pattern with that reported for MOF-801 (***Microstructures 2024;4:2024023***), shown below.

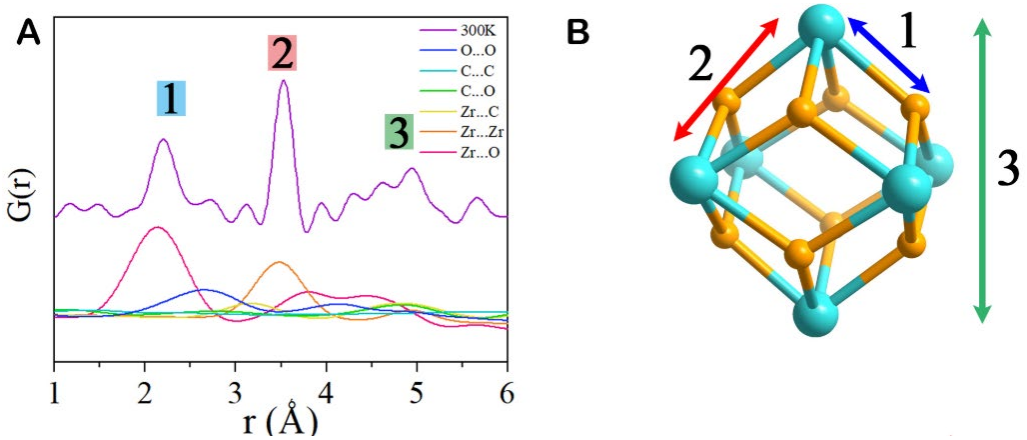

This closely matches the PDF observed for our Zr-FMA MOF, consistent with the presence of Zr_6O_8 oxoclusters that are the characteristic building blocks of Zr-MOF-801:

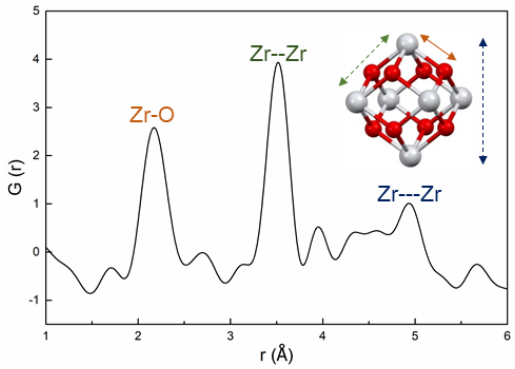

We have added the magnified portion of the PDF to Figure 3C as shown below:

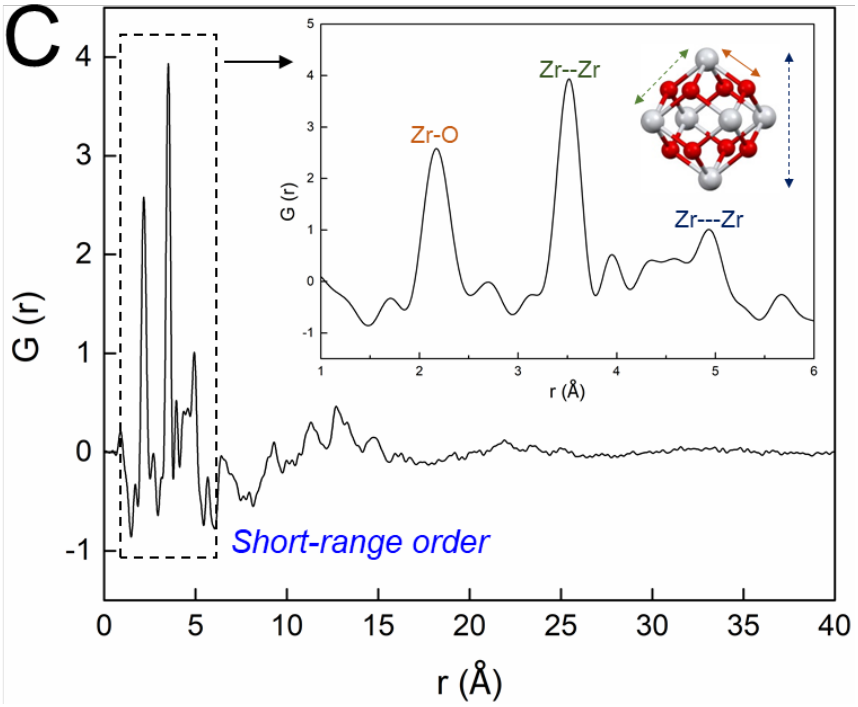

The corresponding explanation and reference have also been added to the manuscript as follows:

Meanwhile, the PDF over a range of 1–6 Å was consistent with that of the typical Zr MOF-801,[40] confirming the local structure of Zr_6O_8 nodes. The inset in Fig. 3c illustrates the interatomic distances for the first 3 peaks of the PDF, in the context of the Zr_6O_8 oxoclusters that are the building blocks of Zr MOF-801.

The mentioned paper was also added in the References:

40. Ma, R. et al. Transition from isotropic positive to negative thermal expansion by local Zr_6O_8 node distortion in MOF-801. *Microstructures* **4**, 2024023 (2024).

In addition, based on the Reviewer's suggestion, we measured the TGA of amorphous Zr FMA in air, which exhibited the similar mass loss to that of the typical crystalline Zr MOF-801, confirming the consistency in stoichiometry. The TGA analysis in air has been added as Figure S16 in the Supplementary information as follows:

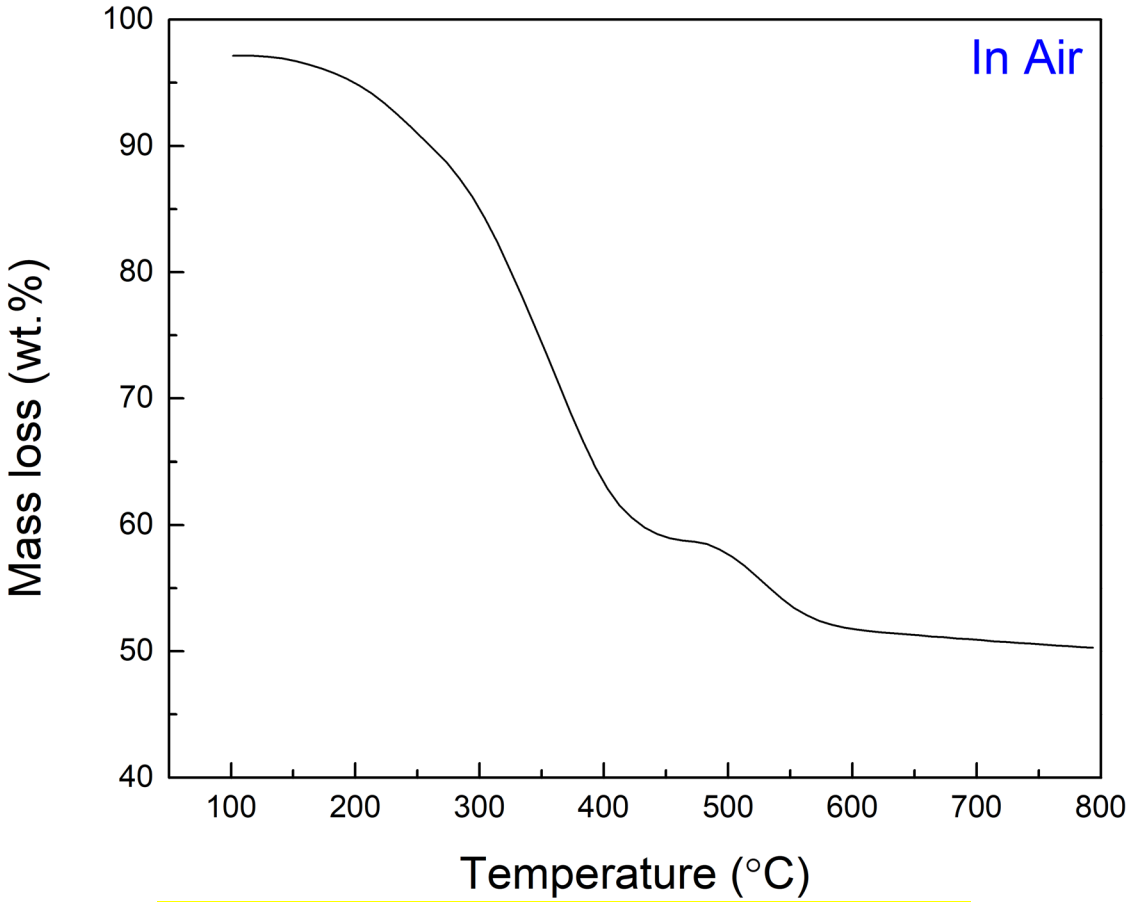

Fig. S16. TGA analysis of amorphous Zr FMA MOF in air.

This can be compared to the TGA presented in Ref. 42:

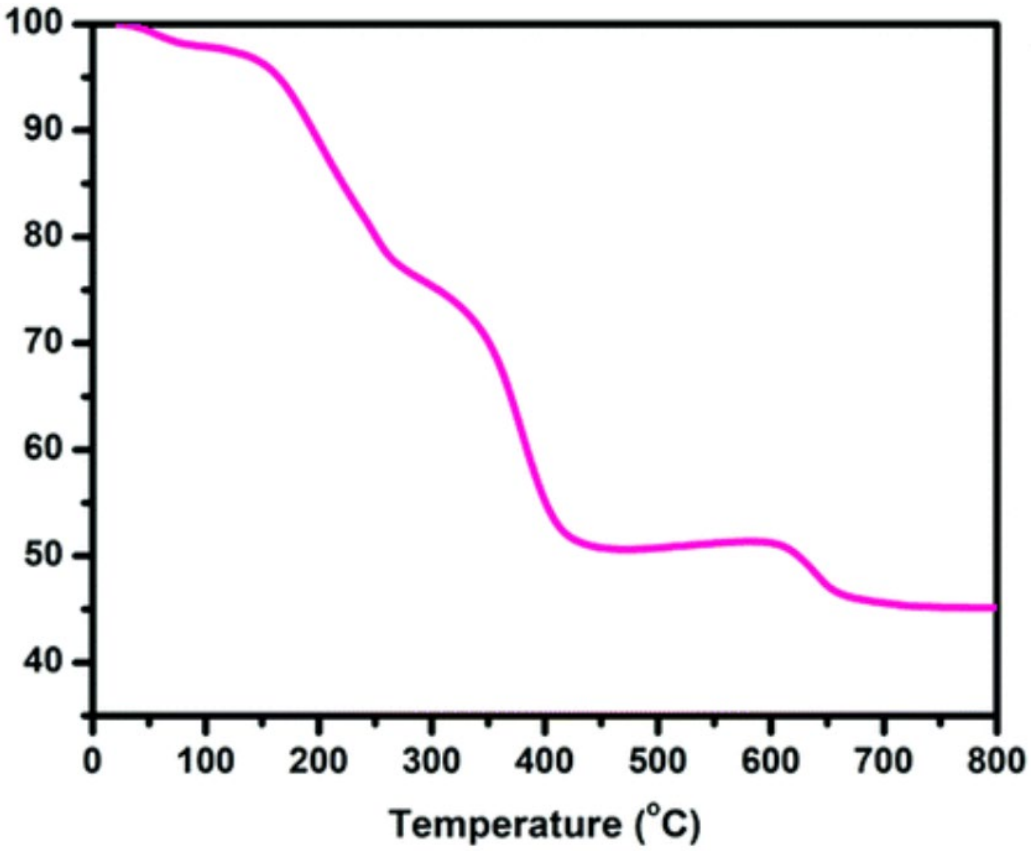

The corresponding explanation and reference have also been added to the manuscript as follows:

The TGA analysis of amorphous Zr FMA in air (**Fig S16**) showed a similar mass loss to that of the typical crystalline Zr MOF-801,[42,43] consistent with the similar stoichiometry.

The mentioned papers are also added in the References:

42. Liu, H. et al. Investigation on a Zr-based metal-organic framework (MOF-801) for the high-performance separation of light alkanes. *Chem. Commun. (Camb)* **57**, 13008-13011 (2021).

43. Muthu Prabhu, S., Kancharla, S., Park, C.M. & Sasaki, K. Synthesis of modulator-driven highly stable zirconium-fumarate frameworks and mechanistic investigations of their arsenite and arsenate adsorption from aqueous solutions. *CrystEngComm* **21**, 2320-2332 (2019).

Finally, as we have shown in the manuscript, the XPS and FTIR spectra of Zr FMA are also consistent with those of the typical Zr MOF-801. All the evidence indicates that the flame-synthesized Zr FMA is an amorphous structure that exhibits short-range order corresponding to Zr_6O_8 nodes like those in MOF-801. Therefore, we believed that the flame-synthesized Zr FMA is an amorphous MOF.

5/ Similar questions must be discussed for the other compounds (Zr UiO-66-NH_2, Fe FMA, 227 Mg DHTA, Cu DHTA, Zr BTC, Zr BPDC, Fe BDC-NH_2 and Hf NDC). Giving the PXRD of the amorphous solids and electron microscopy images of the particles is clearly not enough to claim the synthesis of an amorphous MOF.

Our response: While we are not able to provide and analyze PDFs for all of these materials, we note that besides XRD, evidence supporting the formation of the amorphous MOFs is provided by Fourier-transform infrared (FTIR) spectroscopy. This technique reveals the formation of coordination bonds between the clusters and the organic linkers, which are absent in the reactants (***Angew. Chem. Int. Ed. 2023, 62, e202300003***). New bonds that are not present in the reactants appears in the MOFs. In the revised SI, we now include the FTIR spectra of all the amorphous MOFs and their reactants, as shown in Figure S18:

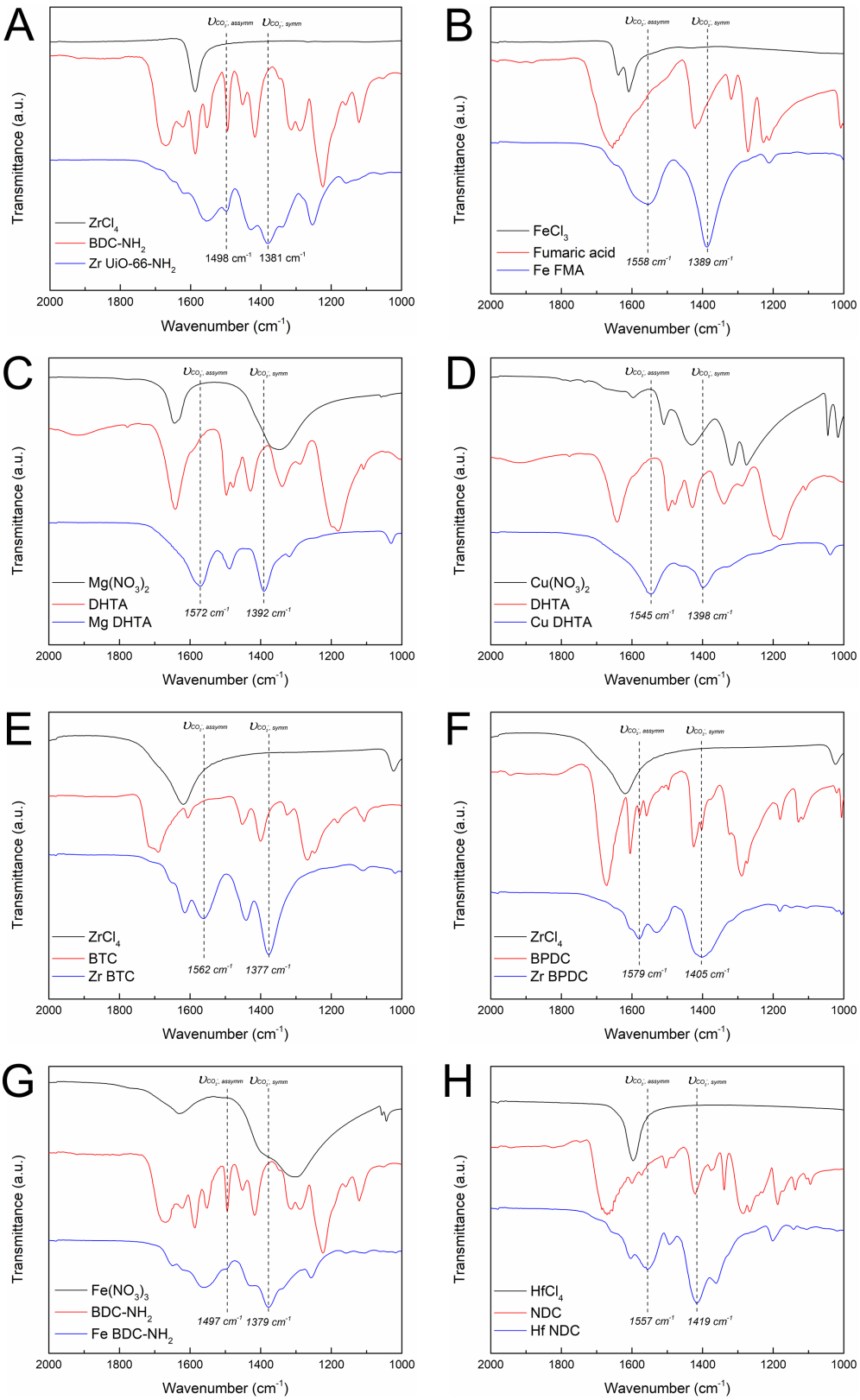

Fig. S18. FTIR spectra of amorphous MOFs **A.** Zr UiO-66-NH_2; **B.** Fe FMA; **C.** Mg DHTA; **D.** Cu DHTA; **E.** Zr BTC; **F.** Zr BPDC; **G.** Fe BDC-NH_2 and **H.** Hf NDC, as well as their reactants.

It is evident that in all the MOFs, new chemical bonds have formed in comparison to their reactants. This demonstrates that in all the amorphous MOFs, the metal ions (nodes) have

successfully coordinated with the organic ligands. Combined with the XRD results, we are confident that all these MOFs possess an amorphous structure along with the metal-ligand coordination expected in the MOFs.

We have added the explanation of FTIR spectra in the manuscript as follows:

Meanwhile, the FTIR spectra of all the amorphous MOFs showed formation of new bonds compared to their reactants (**Fig. S18**), demonstrating coordination between the clusters and the organic linkers.[45]

The mentioned paper is also added in the References:

45. Xu, W. et al. High-Porosity Metal-Organic Framework Glasses. *Angew. Chem.-Int. Edit.* **62**, e202300003 (2023).

In addition, based on the Reviewer's suggestion, we also compared the PDF pattern of flame-synthesized amorphous Zr UiO-66-NH_2 to the PDF patterns of previous reported crystalline and amorphous UiO-66 MOFs:

In the reference (***Physical Chemistry Chemical Physics 18.3 (2016): 2192-2201***), the PDF patterns of the crystalline and amorphous UiO-66 MOFs are shown as follows. It can be observed that at short-range distances, the PDF patterns of the two MOFs are consistent. However, with increased distance, distinct peaks are still visible in the crystalline UiO-66 MOF, while the peaks in the amorphous UiO-66 MOF gradually disappear.

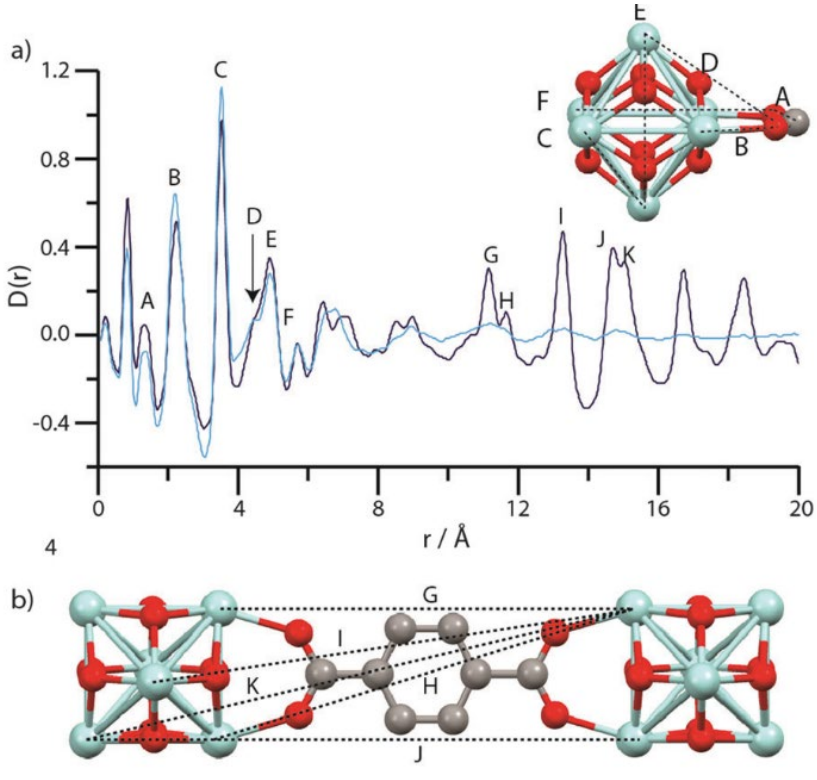

In this study, our PDF pattern of the amorphous UiO-66-NH_2 was as shown below. Like the amorphous MOFs reported in the literature, the peaks gradually disappear at mid-range distances. At short range, the positions of the peaks are consistent with those reported in the literature, confirming the presence of Zr_6O_8 clusters.

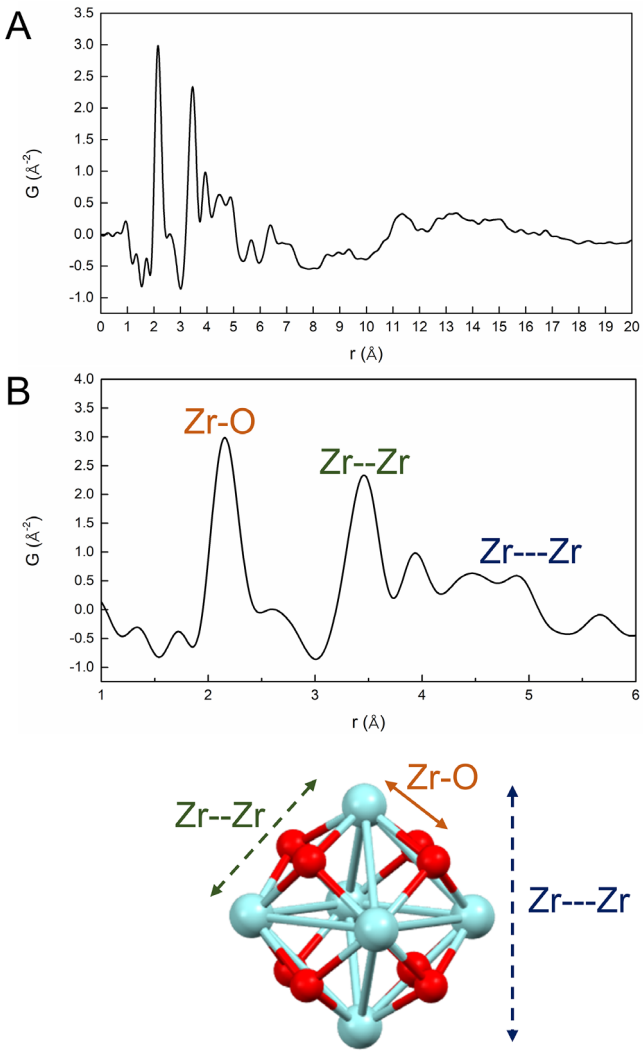

Fig. 23. Zoomed-in PDF patterns of the Zr UiO-66-NH_2 MOF in the 0–20 Å and 0–6 Å regions.

We have added the explanation of the amorphous UiO-66-NH_2 PDF pattern in the manuscript as follows:

The PDF pattern in the medium distance range of 0–20 Å (**Fig. S23A**) was consistent with the previously reported amorphous Zr UiO-66 MOF. At shorter range of 1–6 Å (**Fig. S23B**), the pattern is consistent with both crystalline and amorphous Zr UiO-66 MOFs.[46] This confirms the amorphous nature of the flame-synthesized UiO-66-NH_2 MOF and the presence of Zr_6O_8 clusters as its building-blocks.

The mentioned literature is also added in the References:

46. Bennett, T.D. et al. Connecting defects and amorphization in UiO-66 and MIL-140 metal-

organic frameworks: a combined experimental and computational study. *Phys. Chem. Chem. Phys.* **18**, 2192-201 (2016).

6/ Authors claim that they can control the amount of Au, Co, Pt, and Pd loaded in the different MOFs but how does the amount of metal cations loaded determined by ICP compare with the expected one. Moreover, did the authors optimize the washing of the doped solids? Did they observe any metal leaching during the washing procedure?

Our response: Based on the Reviewer's suggestion, we measured the metal ratios in the MOF products by ICP and compared to the metal ratios designed in precursor. The results are shown in Table S13 as follows:

Table S13. ICP analysis of the doped metals in MOFs

Bi-metallic MOFs	Designed in precursor (M_1:(M_1+M_2) in mol.)	ICP measured in product (M_1:(M_1+M_2) in mol.)
Au-Cu HKUST-1	0.050	0.026
Co-Ni PBA	0.100	0.106
Pt-Zr UiO-66-NH_2	0.100	0.074
Pd-Zr FMA	0.100	0.081

The composition ratio of Co and Ni in Co-Ni PBA remains consistent with that in the precursor. This consistency can be attributed to the similar properties of Co and Ni and the identical crystal structure of their respective PBAs, which preserve the elemental ratio from the precursor to the final product. Conversely, in other MOFs, significant differences in the properties of the metal elements can cause deviations in their ratios in the final product compared to the precursor, particularly under rapid, non-equilibrium synthesis conditions.

We have added the explanation in the manuscript as follows:

The molar ratios of the two metals in the bi-metallic MOF products are shown in **Table S13**. Given that Co and Ni share similar properties and both Co PBA and Ni PBA exhibit the same cubic FCC structure, the Co-Ni PBA exhibited an elemental ratio in the final product very close to that in the precursor solution. However, in other bi-metallic MOFs, due to the differences in the physicochemical properties of the two metal elements, the ratio of elements in the final product deviated from the ratio provided in the precursor.

Additionally, the washing procedure was the same as that used for both single-metallic crystalline and amorphous MOFs. Thus, the doped metal remains stable in the MOF matrix. As shown in **Figure 5** and **Figure S35**, a strong reducing agent ($NaBH_4$) is required to extract the noble metal from the MOF matrix, which then forms highly dispersed and stable nanoparticles on the MOF surface rather than leaching into the solution. Therefore, regular washing procedures cannot leach out the doped metals.

7/ Finally, the authors should carefully check the reference list. Some of them seems to be completely unrelated to the citation. For example « Additionally, the particular surface characteristics of these nano-crystals may lead to enhanced reactivity and selectivity in chemical reactions" is not related to reference 18 "Introduction to metal-organic frameworks" that is a very broad introduction on MOFs and "Moreover, the higher concentration of structural defects in nano-crystalline MOFs can be beneficial." is not related to reference 19 whose title is "Weaving of organic threads into a crystalline covalent organic framework" that deals with COFs and not MOFs.

Our response: Thank you very much for this reminder. Based on the Reviewer's suggestion, we have carefully checked the references list. All the references in the current manuscript are closely related to the cited sections. The references 18 and 19 have been corrected to the following:

18. Barros, B.S., Neto, O.J.D., Fros, A.C.D. & Kulesza, J. Metal-Organic Framework Nanocrystals. *ChemistrySelect* **3**, 7459-7471 (2018).

19. Dai, S. et al. Highly defective ultra-small tetravalent MOF nanocrystals. *Nat. Commun.* **15**, 3434 (2024).

Response to Reviewer #3's comments:

Reviewer #3 (Remarks to the Author):

The manuscript describes the non-equilibrium gas phase synthesis of crystalline/non-crystalline metal organic framework architectures. I find this process idea fascinating and worth publishing in nature communications. The success of this technique would significantly contribute to the synthesis of these classes of materials that are possible only via multiple chemical routes as shown in scheme 1. However, before this manuscript can be published, there are some critical chemical engineering issues during synthesis that need to be clarified.

We thank the Reviewer for the positive comments!

1. The H_2 and O_2 combustion in an inverted diffusion flame was realized with additional 10L/min N_2-Co flow to cool down the flame. While the stoichiometry of H_2/O_2 ratio for complete combustion is 1/0.5 [$H_2 + 0.5O_2 = H_2O + (-470kJ/mol)$], the ratio used in the manuscript is 1/1.14 ($3.5LH_2/4LO_2$ min^{-1}), i.e. highly O_2 rich environment. The reaction is exothermic with extra surplus oxygen. As authors suggested, the temperature of the reactor is maintained at 400°C is highly unlikely due to easy exothermic oxidation resulting to more heat generation in the reaction vicinity. As shown in figure 1, the high flow of N_2 (140L/min) would cool down the aerosol stream but the high temperature in the reaction zone would decompose the precursor components, that depends on flame top -precursor entry point distance. What is the distance from the top of the flame to the precursor entry point? If the aerosol stream is already around 400°C, why is there a need of such a high N_2 co-flow?

Our response: The distance from the top of the flame to the precursor entry point is ~5 cm. As shown in Figure 1 and Figure S1, MOF particles formed in the reactor chamber and were subsequently quenched in the quenching chamber by a high flow of N_2 (140 L/min). The 10 L/min N_2 flow is provided to ensure a suitable total flow rate for achieving sonic velocity in the nozzle downstream of the flame, which promotes atomization of the liquid precursor within the nozzle. The total flow rate also determines the residence time (~50 ms) of the MOF product in the high-temperature environment of the chamber. The temperature achieved in the reactor is significantly lower than the adiabatic flame temperature due to cooling upon expansion through the nozzle, cooling due to evaporation of the precursor, and losses to the surroundings by conduction and radiation. The 140 L/min of N_2 downstream serves to rapidly quench the MOF

product formed in the reactor chamber, preventing the aggregation of MOF particles. More importantly, as reported in our previous study on preparing immiscible solid solutions (***S. Liu et al., Nature Communications 15.1 (2024): 1167***), high flow rate N_2 quenching preserves the metastable structures of products formed at high reaction temperatures. This mechanism is also applicable to the synthesis of metastable bi-metallic MOFs, as we described in the **Figure 4** section.

We have added the role of the co-flow N_2 in the Methods section as follow:

Nitrogen supplied to the flame along with the hydrogen fuel serves increase the overall gas flow rate and limit the peak flame temperature. The overall gas flow rate should be high enough to achieve sonic velocity within the nozzle that separates the flame from the reaction chamber. The overall gas flow rate also determines the residence time of the MOF product in the high-temperature reaction chamber. Note that the temperature in the reaction chamber is far below the adiabatic flame temperature due to heat losses to the surroundings as well as cooling due to expansion and precursor solution evaporation.

2. The components for Cu-based MOF (Cu HKUST-1) described in the text are $Cu(NO_3)_2$ and 1,3,5-benzenetricarboxylic acid, DMF, EtOH, and H_2O.

• Out of these components, $Cu(NO_3)_2$ decomposes at ~400°C. In this case, how would Cu be incorporated in the organic framework?

• 1,3,5-benzenetricarboxylic acid, DMF, EtOH decompose at 250, 350 and 78°C, i.e. each component has different temperature of decomposition. While the process is very rapid, how would the time be sufficient for different decomposition components followed by the MOF formation?

Our response: Although the MOF formation process occurs within aerosol droplets, the MOF precursors start out dissolved in solution. Thus, the $Cu(NO_3)_2$ is present as Cu^{2+} and NO_3^- ions in the precursor solution. Likewise, the BTC is dissolved in partially or fully deprotonated form. Thus, the MOF formation does not require decomposition of these precursors or their evaporation into the gas phase. Rather, it requires that the BTC ligands coordinate to the Cu^{2+} ions. This happens rapidly as the solvent evaporates. The byproduct (nitric acid) evaporates along with the solvents at temperatures below the reactor temperature. We have attempted to illustrate this schematically in Figure 1. Initially, atomization of the precursor solution forms precursor microdroplets in the reaction chamber, each droplet serving as a microreactor, containing Cu^{2+} cations, BTC linkers, and solvents. At high temperature, the solvent in the droplets evaporates. During the evaporation process, the concentrations of the Cu cations and

BTC linker increase. As a result, Cu ions coordinate with BTC linkers to form the MOF structure.

The production of numerous MOF nanocrystal domains in an overall hollow sphere structure provides evidence of this evaporation-driven mechanism. As the solvent evaporates from the surface of the droplet, the solute concentrations are higher at the surface than at the center, causing the MOF to initially nucleate at the surface of the droplet and then grow inward, ultimately creating a hollow structure. This evaporation-driven droplet-to-particle process also can be applied to produce other porous materials. For example, in our previous study (***S. Liu et al., Angewandte Chemie 134.35 (2022): e202206870***), mesoporous silica was fabricated in a flame reactor *via* a micelle self-assembly process during the droplet-to-particle conversion.

The entire droplet evaporation process occurred within a few milliseconds (***Drying Technology 27.1 (2009): 3-13***), which is still sufficient for MOF coordination. This rapid formation is the key point that distinguishes this method from conventional equilibrium synthesis approaches. Because the MOF forms very quickly, it does not have enough time to grow into large single crystals like those MOFs produced by traditional solvothermal methods. Instead, it enables the formation of novel, kinetically stabilized poly-nanocrystalline MOFs, amorphous MOFs, and metastable bi-metallic MOFs.

Final revision

Reviewer #1 (Remarks to the Author):

All issues have been well addressed point by point. It can be accepted for publication in Nature Communications.

We appreciate the reviewers' suggestions and support for this study.

Reviewer #2 (Remarks to the Author):

The authors satisfactory took into account all the issues raised in my previous report. Therefore, I recommend the publication of the manuscript in its current form.

We appreciate the reviewers' suggestions and support for this study.

Reviewer #3 (Remarks to the Author):

The manuscript describing the non-equilibrium gas phase synthesis of crystalline/non-crystalline metal organic framework architectures has been nicely revised. The reviewer questions (from all the three) from the manuscript are well clarified. I believe that this manuscript is now ready for the publication in nature communications.

We appreciate the reviewers' suggestions and support for this study.

One last question: Authors claim “HNO_3 (as a byproduct) evaporates along with the solvents”.

• What is the boiling point difference between nitric acid and the other solvents?

• Does HNO_3 decompose during the process?

• What are the safety issues for non-exposure conditions to the environment?

Please clarify this in the final version.

Our response: In fact, the amount of nitric acid produced in the reaction is very small compared to the overall solvent content, so its boiling point is very close to that of the solvent. Meanwhile, at high temperature, nitric acid will immediately decompose into a small amount of NO_2 gas,

which is expelled along with other gases. Non-exposure conditions are safer. For example, the harmful gases generated in the reaction are discharged into the fume hood rather than being directly released into the air, thus eliminating the risk to human health. It also prevents the exposure of flames to the air and the dangers caused by fuel leakage. No safety issues have ever occurred with this reactor. We have clarified these points in the Methods section in the final version of the manuscript.